Delamination Assessment in Composite Laminates through Local Impulse Excitation Technique (IET)

applied sciences

MDPI

Article

Delamination Assessment in Composite Laminates through Local Impulse Excitation Technique (IET)

Carlo Boursier Niutta [1], Pierpaolo Padula [1], Andrea Tridello [1], Marco Boccaccio [2], Francesco Acerra [3] and Davide S. Paolino [1,*]

[1] Department of Mechanical and Aerospace Engineering, Politecnico di Torino, 10129 Turin, Italy; carlo.boursier@polito.it (C.B.N.); pierpaolo.padula00@gmail.com (P.P.); andrea.tridello@polito.it (A.T.)
[2] Leonardo Labs, OGR Tech, 10138 Turin, Italy; marco.boccaccio.ext@leonardo.com
[3] Leonardo Aircraft Division, 80038 Pomigliano d'Arco, Italy; francesco.acerra@leonardo.com
* Correspondence: davide.paolino@polito.it

Abstract: This paper deals with an innovative nondestructive technique for composites (local-IET), which is based on the Impulse Excitation Technique (IET) and, in the presence of damage, assesses the degradation of the elastic properties of a local region of the laminate by reversibly clamping its boundaries. In this paper, a numerical analysis of the sensitivity of the local-IET to the delamination damage mechanism is conducted. Firstly, a Finite Element (FE) model of the local-IET test is determined through experimental investigations on undamaged composite laminates, which cover a wide range and are made of glass or carbon fibers, through resin infusion or pre-preg consolidation and with unidirectional or fabric textures. The vibrational response of a glass fiber composite with local delamination is then assessed with the local-IET. By modeling the delamination in the simulation environment, the effectiveness of the FE model in replicating the vibrational response, even in the presence of delamination, is shown through a comparison with the experimental results. Finally, the FE model is exploited to perform a sensitivity analysis, showing that the technique is able to detect the presence of delamination.

Keywords: laminated composites; damage assessment; delamination; local Impulse Excitation Technique

Citation: Boursier Niutta, C.; Padula, P.; Tridello, A.; Boccaccio, M.; Acerra, F.; Paolino, D.S. Delamination Assessment in Composite Laminates through Local Impulse Excitation Technique (IET). *Appl. Sci.* **2024**, *14*, 3023. https://doi.org/10.3390/app14073023

Academic Editor: Manoj Gupta

Received: 7 March 2024
Revised: 25 March 2024
Accepted: 27 March 2024
Published: 3 April 2024

1. Introduction

In recent decades, there has been an increasing demand for composite materials in the industrial landscape. Composite materials satisfy the need for lightweight yet highly performing materials with fiber-reinforced materials, which have demonstrated abilities to have a flexible design and be used in almost every type of industrial application. Also, composites are characterized by enhanced damage tolerance with respect to standard metal alloys.

However, the wide application of composite materials still has limitations due to the lack of proper strategies for damage quantification. Due to their mixed compositions and the large difference between the fiber and matrix properties, composite materials present several damage mechanisms, each affecting a specific scale, such as fiber breakage and matrix cracking at the micro-scale or delamination at the laminate scale, which demand accurate and local investigations. As the damage determines a degradation in macro-scale material properties, several nondestructive techniques (NDTs) have focused on the assessment of the damage and its severity by investigating the material's macro-scale response. Among these, we can mention ultrasonics [1,2], acousto-ultrasonics [3,4], acousto-ultrasonics in combination with neural network algorithms [5,6], the Detecting Damage Index [7], thermography [8–10], resistivity-based measurements [11–14] and optical methods, such as Shearography and Digital Image Correlation [15,16]. The reader can refer to [17] for details on the advantages and limitations of each NDT. Although they

provide quantitative information on the damage severity as a degradation of the elastic, thermal, or electrical response of the material, a main drawback of these methodologies is the cost related to the complex equipment needed for each technique. Furthermore, it is usually necessary to transport the component to a specific location for nondestructive tests, which further increases the costs.

The authors have recently proposed an NDT based on the Impulse Excitation Technique, which aims to determine the local variation in the elastic properties of the damaged region of a composite component (local-IET) [18–20]. By reversibly clamping its extremities through a vacuum, the vibrational response of the inspected region is isolated, with the measured resonant frequencies only being a function of the elastic characteristics of the investigated area. This allows for the sensitivity of the vibrational test to be enhanced in the presence of local damage [20]. Furthermore, from the local vibrational response, the local variation in the elastic properties can be assessed, and the damage severity is quantified in terms of the degradation of the elastic properties. Since it is a vibrational test, the equipment of the local-IET has a relatively low cost, and the methodology allows for on-site analyses of composite components with a significant cost reduction [17,18,20].

This paper aims to investigate the sensitivity of a local-IET in the presence of delamination. Delamination, i.e., the debonding between adjacent laminae, is among the most critical damage mechanisms of a composite as it prevents the transfer of forces and moments between plies, thus affecting the strength of the laminate. For example, under compressive loads, buckling instability is likely to occur if the delaminated ply has a free surface on one side [21]. Delamination can occur both during the manufacturing process, as contaminations due to dirt cause poor bonding between laminae [22,23], and during the in-service life of the component. Under fatigue loads, delamination occurs as matrix cracks lengthen with the cycles and interact with each other. Under lateral loading, as in the case of impact loads, delamination is caused either by interlaminar stresses due to bending or by matrix cracks in proximity of plies interfaces [24]. As such, the proper identification of the presence of delamination within a composite component is crucial for a health state assessment. Zak et al. [25] recently showed that vibrational methods can be successfully adopted for delamination detection. They performed experimental and numerical investigations on composite beams and plates clamped at one side and delaminated at the other, with different ratios of delamination length with respect to the total structure length. The results show a reduction in the resonances with an increasing delamination size. For example, for delamination with length corresponding to 30% of the structure length, the reduction in the resonance frequencies was about 5%. It is worth noting that by investigating the global vibrational response, both the delaminated and undamaged portions of the material participate in the vibrations, thus limiting the sensitivity only to high-level damage. By confining the vibrational response only to a region of interest as in the local-IET, the presence of damage can be more easily detected.

In this paper, the goal is to assess the sensitivity of a local-IET in the presence of delamination within the inspected region through Finite Element (FE) analyses. The FE model of the local-IET test has been identified through a modal displacement analysis on undamaged composite laminates to replicate the boundary conditions provided by the isolating device. The vibrational response of a glass fiber composite with local delamination has been experimentally assessed with the local-IET and compared to the FE results to validate the numerical model. Finally, the FE model has been exploited to perform a sensitivity analysis, where the size of the delamination, its location within the device and position of the impulse are investigated.

2. Materials and Methods

In this section, the material properties of the investigated composite laminates are first presented. The experimental setup is then detailed, highlighting the main aspects that must be accounted for in the FE model, whose details are provided at the end of the section.

2.1. Materials

The composite plates adopted in the present work cover a wide range and involve composite laminates made of glass or carbon fibers through resin infusion or pre-preg consolidation and with unidirectional or fabric textures. In total, five different laminates have been retained: (i) a unidirectional carbon fiber, (ii) a plain weave carbon fiber, (iii) a twill 2 × 2 carbon fiber, (iv) a twill 2 × 2 pre-preg glass fiber, (v) a twill 2 × 2 glass fiber made by vacuum bag infusion. All of the laminated plates had dimensions of at least 300 × 300 mm.

The unidirectional and plain weave were carbon fiber composites and were manufactured by HP Composites (Ascoli Piceno, Italy) in autoclave from pre-preg. The unidirectional plate was made of 8 layers stacked in the same direction (stacking sequence $[0]_8$) and had a total thickness of 0.96 mm. The plain weave was made of 4 layers, each 0.24 mm thick and all stacked with the same orientation.

The third retained material was an 8-layer twill 2 × 2 carbon fiber, with the commercial name XC110, stacked in the same direction and pre-impregnated with epoxy resin. The curing cycle was accomplished in an oven at 120 °C for 8 h. The consolidated thickness was 1.8 mm.

The fourth and fifth materials were made of glass fibers. The fourth was made of 4 layers pre-impregnated with epoxy resin with a total plate thickness of 2.1 mm. The material was cured in an oven under a vacuum at 120 °C for 8 h. The glass fabric of the fifth material was twill with dimensions of 2 × 2, made of E-glass fibers, whose concentration in the warp and weft directions is almost equivalent. The epoxy resin, commercial name EP-IN2-S-5, was vacuum-infused, and the plate was cured under a vacuum for 24 h and post-cured in an oven at 100 °C for 3 h. The plate had a consolidated thickness of 1.2 mm. The fifth material also presented a delaminated zone, whose geometry can be approximated as a circle with a diameter of 50 mm, as shown in Figure 1.

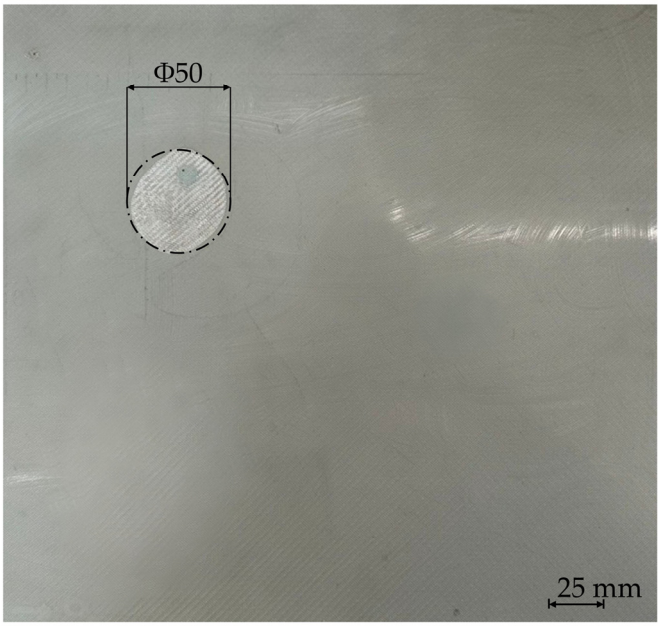

Figure 1. Example of local delamination in 8-layer glass fiber composite.

Delamination was induced through a water jet machine by spreading a release wax film in the middle of the laminate, i.e., between the fourth and the fifth layers, before the resin infusion, which prevented the local adhesion of the resin to the glass fabric. When water jet cutting the plate in correspondence to the wax film, the high-pressure water encountered a discontinuity in the matrix phase, which facilitated the propagation of the water in the in-plane direction, thus inducing the delamination.

Table 1 reports the material properties of the laminates in accordance with the main material directions.

Table 1. Material properties of = investigated composite plates assessed through IET tests.

Property [Unit]	Unidirectional Carbon Fiber Plate—MAT#1	Plain Weave Carbon Fiber Plate—MAT#2	Twill 2 × 2 Pre-Preg Carbon Fiber—MAT#3	Twill 2 × 2 Pre-Preg Glass Fiber—MAT#4	Resin Infused Twill 2 × 2 Glass Fiber—MAT#5
Density [g/mm^3]	1.57	1.46	1.43	1.82	1.65
Thickness [mm]	0.96	0.96	1.8	2.1	1.2
E_1 [GPa]	153.2	46.5	51.1	24.0	19.0
E_2 [GPa]	9.2	46.5	51.1	24.0	18.6
G_{12} [GPa]	5.2	4.0	3.9	5.2	3.6
ν_{12} [-]	0.35	0.08	0.08	0.2	0.17
Tsai modulus [GPa]	174.0	101.6	110.7	60.4	45.9
TrD [kN·mm]	12.83	7.49	54.92	47.28	6.60

The dynamic elastic properties were determined through flexural and torsional IET tests in accordance with the ASTM standard E1876 [26]. Bar specimens of 20 × 100 mm were cut from the plates using the water jet machine. Table 1 also reports the Tsai modulus and the trace of the flexural matrix $[D]$ of each material [27], which are considered to account for the material elasticity. The first four materials were used to calibrate the FE model of the local-IET test, while the fifth material was used for validation.

2.2. Local-IET Setup and Test

The local-IET adopts a specific device which clamps the boundaries of the region of interest through a vacuum and confines the mechanical vibrations in the region comprised within the device. The vibrational response is thus only a function of the material properties of the investigated region, which strongly enhances the sensitivity of the vibrational test in the presence of local damage.

The device has a frame shape with an external seal and an internal seal delimiting the zone vacuumed through a pump. The vibrational response of the region comprised within the internal seal is detected. At the end of the test, a shut-off valve facilitates the removal of the clamped plate. Figure 2 shows the four devices adopted in this work.

The devices are characterized by different dimensions of the investigated region, namely 50 × 50, 75 × 75, 100 × 100 and 150 × 150 mm. The first three devices are made of 3D-printed polyethylene terephthalate, while the 150 × 150 mm device is made of an aluminum alloy and produced by CNC machining, as the dimensions are incompatible with the 3D-printer. No influence of the device material can be expected with the laminates being in contact with the rubber seals. The devices are fixed to a working table, that is, one side of the composite plate is clamped with the device and, on the opposite side, the vibrational response is acquired. However, the setup can be easily converted to adopt the technique on industrial components, where usually only one side of the component can be accessed for non-destructive investigation.

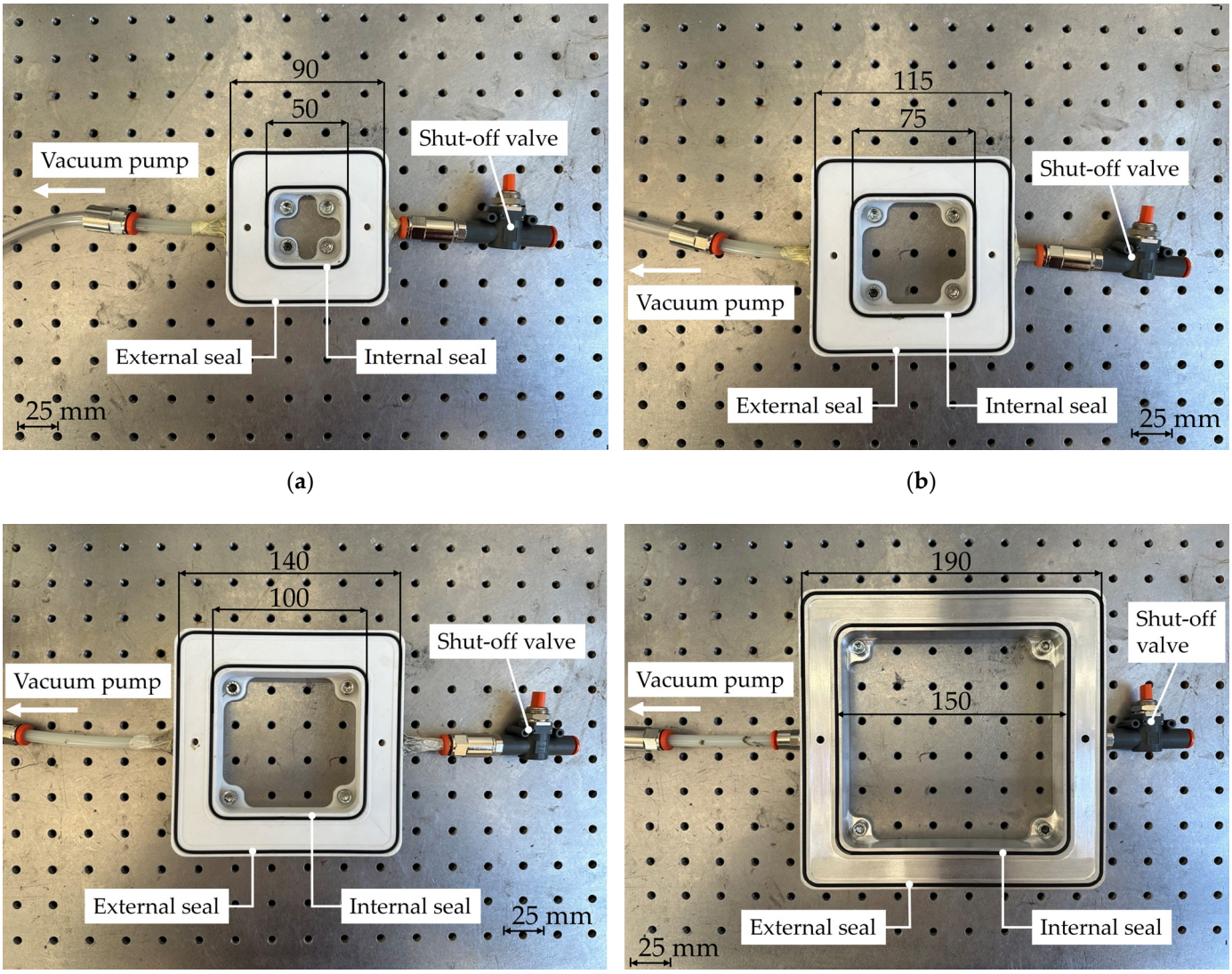

Figure 2. Clamping devices of the local-IET: (**a**) 50 × 50 mm; (**b**) 75 × 75 mm; (**c**) 100 × 100 mm; (**d**) 150 × 150 mm.

According to [20], the confinement of mechanical vibrations to a subregion of the component enhances the sensitivity in the presence of local damage, whose severity has been characterized in [20] in terms of the degradation of the first resonant frequency.

In order to replicate the local-IET test in the FE environment, the vibrational response of the first mode, i.e., the first resonant frequency and the modal displacement of the first mode, was investigated on the undamaged plates. A KEYENCE LK-H022K laser system was employed, which ensures a precise measurement of the out-of-plane displacement. From the displacement data, the first resonance was determined through a Fast Fourier Transform of the signal. Figure 3 shows the experimental setup.

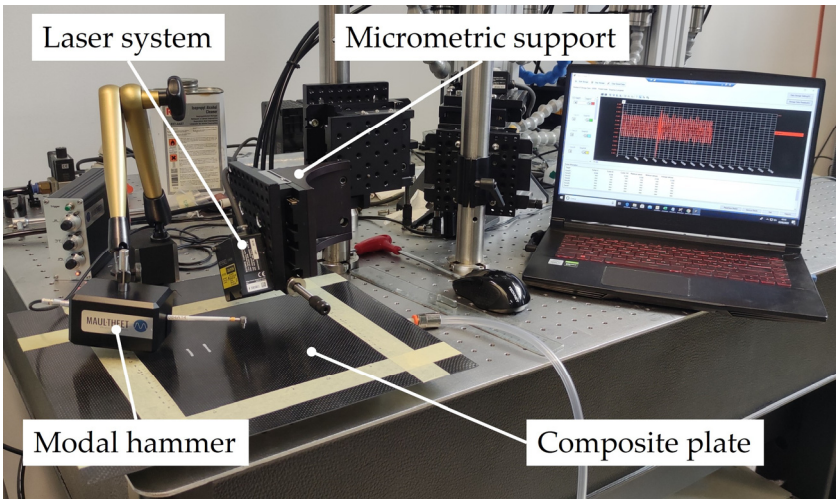

Figure 3. Experimental setup of the local-IET tests for modal displacement investigations.

The impulse was provided through a Maul-Theet Impact HaC-3 modal hammer, which guarantees the same input energy, thus allowing a reliable acquisition of the modal displacement to be obtained.

For the determination of the first resonant frequency, a dedicated MATLAB script was developed, which first filters the acquired signal with a high-pass filter to eliminate the spurious vibrations induced by the vacuum pump, and then transforms the discrete signal in the frequency domain through Fast Fourier Transform. According to Hearmon [28], the first resonant frequency of an orthotropic clamped plate can be written as follows:

$$f = \frac{\lambda}{2\pi} \cdot \sqrt{\frac{1}{\rho \cdot h}} \cdot \sqrt{\frac{D_{11}}{a^4} + \frac{D_{22}}{b^4} + \frac{0.605 \cdot H}{a^2 \cdot b^2}} \tag{1}$$

where]ρ is the material density, h is the plate thickness, a and b are the plate dimensions, and $D11$, $D22$ and H are the flexural stiffness terms, defined as

$$\begin{aligned} D_{11} &= \frac{E_{11} \cdot h^3}{12(1 - \nu_{12} \cdot \nu_{21})} \\ D_{22} &= \frac{E_{22} \cdot h^3}{12(1 - \nu_{12} \cdot \nu_{21})} \\ H &= v_{12} \cdot D_{22} + \frac{G_{12} \cdot h^3}{6} \end{aligned} \tag{2}$$

Considering the square shape of the devices of Figure 2, the formula of Equation (1) was rewritten as

$$f = \frac{\lambda}{2\pi a^2} \cdot \sqrt{\frac{1}{\rho \cdot h}} \cdot \sqrt{TrD} \tag{3}$$

where the flexural stiffnesses were substituted by the trace of the flexural matrix D, which is proportional to the sum of the flexural stiffnesses D_{11}, D_{22} and $\frac{G_{12}}{6 \cdot h^3}$ and to the Tsai modulus of the material through the plate thickness [27].

The λ parameter of Equation (3) defines the boundary conditions of the rectangular plate. Its value ranges from 1 (for simply supported boundaries) to 22.4 (for fully clamped boundaries). As the device aims to isolate the vibrational response, the desired value of λ for vacuum clamping should be as near as possible to 22.4. Therefore, by investigating the λ parameter, the clamping effectiveness, which is the ability of the device to isolate the vibrational response, can be assessed.

The modal displacement of the first mode was acquired with a sampling frequency of 20 kHz. The laser was mounted on a linear micrometric support which allows its position be to precisely adjusted and set. Measurements were acquired along a line with a constant interval between each other. A step size of 10 mm was considered, except for the

50 × 50 clamping device, whose step size was 5 mm. The vertical displacement was also measured in correspondence with the extremities in order to investigate the behavior of the plate in correspondence with the internal seal. For the twill and plain weave laminates, only one measurement line was acquired, given the symmetry of the system. On the contrary, in the case of the unidirectional plate, two measurement lines were considered in order to determine the modal displacements along the two main material directions. It is worth mentioning that, to provide the impulse impact in the center of the investigated region, the measurements of the modal displacement were acquired along a line located between the center and the boundary of the device.

Concerning the fifth material, according to the literature on nonlinear acousto-ultrasonic NDTs [1,29], a relevant factor for the detection of delamination damage in composites is the ratio between the power amplitude of the second resonance frequency A_{mode2} and the squared power amplitude of the first resonance frequency A_{mode1}, thus defined as

$$\beta = \frac{A_{mode2}}{A_{mode1}^2} \tag{4}$$

The β factor is usually referred to as a second-order nonlinear coefficient and represents a measure of the nonlinear behavior of the material in the presence of damage. In particular, due to the nonlinearities, the participation of the second mode and, accordingly, the β factor increases in the presence of damage.

For the experimental investigations, the delamination was positioned in the center of the 100 × 100 mm device. The impact was provided at 10 mm from the center of the inspected region, and the Frequency Response Function (FRF) was computed along a line parallel to one of the boundaries of the device and at a distance of 20 mm from the center with a step size of 5 mm, as shown schematically in Figure 4.

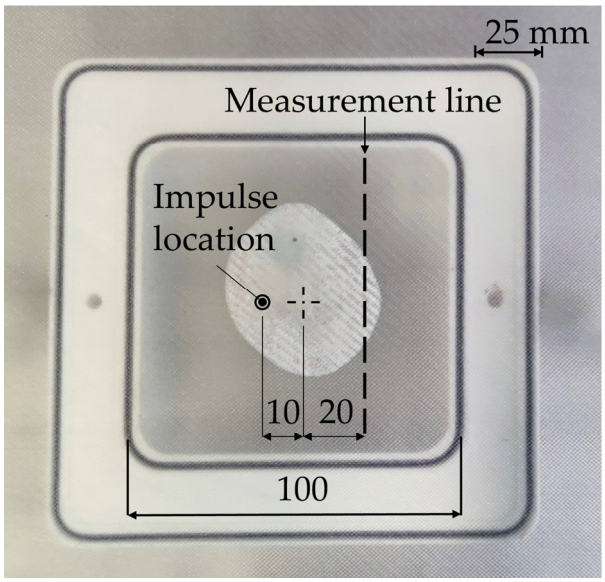

Figure 4. Impulse position and measurement line for experimental investigation of delamination with local-IET.

At least three repetitions for each investigated point were considered. The experimental response was also investigated in the undamaged side of the composite plate, and the ratio $\frac{\beta_{dam}}{\beta_{undam}}$ between the damaged and undamaged β factors was retained to evaluate the effectiveness of the FE model. Because it increases as the contribution of the second mode increases due to the damage, the ratio $\frac{\beta_{dam}}{\beta_{undam}}$ was also considered to evaluate the sensitivity of the local-IET in the presence of delamination.

2.3. Finite Element Model of Local-IET

The local-IET test was replicated in an LS-Dyna environment through a modal analysis. To compute the power amplitude of the first resonance frequency A_{mode1} and the power amplitude of the second resonance frequency A_{mode2}, the FRF due to nodal excitation was computed by considering a damping ratio coefficient ζ equal to 0.002 as a result of the logarithmic decrement determined in the IET tests of the bar specimens.

Four nodes of Belytschko-Tsai shell elements with one integration point for each layer of laminate were used with a mesh size of 1 mm, according to a convergence analysis [18], to model the region within the internal seal. The *PART_COMPOSITE keyword was exploited to build the material stacking sequences. All of the retained materials were modeled with an elastic orthotropic material law (*MAT_ORTHOTROPIC), whose material properties are reported in Table 1. For the specimen with delamination, two layers of shells, each composed of half of the total laminate plies, were modeled and connected through solid adhesive elements to simulate the matrix phase. In correspondence with the delamination, the elements were removed, thus preventing any transfer of forces or moments between the two layers. The material behavior of the resin was assumed to be a linear isotropic elastic (*MAT_ELASTIC), whose properties were taken from [30].

Ideally, the extremities of the investigated region are perfectly clamped, which assures the isolation of the mechanical vibration [18]. In order to ensure that the actual boundary conditions can diverge from the ideal clamping, two FE approaches were pursued here, both involving springs at the extremities. In the first approach, the out-of-plane displacement was released and governed by the stiffness of the translational springs, which aim to replicate the noninfinite stiffness of the internal seal. In the second approach, in order to simulate the boundary conditions between the simply supporting and the clamping conditions, the in-plane rotational degrees of freedom were released and governed by the stiffness of the rotational springs.

Figure 5a shows the FE model for the undamaged plate and with the boundaries simulated with springs at the extremities. Figure 5b shows the FE model developed for the simulation of the delamination.

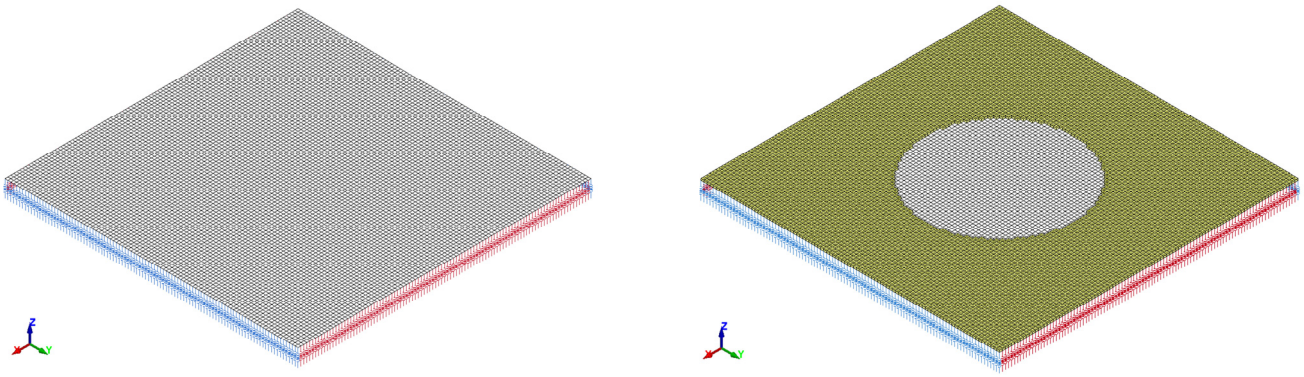

(**a**) (**b**)

Figure 5. The FE model of the local-IET test: (**a**) springs at the extremities to replicate the compliant constraint provided by the seal of the local-IET device; (**b**) the FE model for the delaminated plates.

LS-Dyna allows for the type of springs to be specified, i.e., translational or rotational, through a dedicated card variable [31,32]. Furthermore, the degree of freedom affected by the spring can be specified through a vector defined with respect to the global reference system [31]. Therefore, according to Figure 5, in the case of the rotational springs model, the red springs affect the rotation around the x axis, and the blue springs govern the rotation around the y axis.

For both FE approaches, the stiffness of the springs was identified for each configuration of material and device by considering the first resonant frequencies acquired on the

undamaged plates. The FE model that better replicates the local-IET test was identified by comparison with the acquired modal displacement of the first mode. Finally, a relationship between the spring stiffness and the main parameters affecting the vibrational response was identified with an optimization process, which was used to compute the stiffness of the springs for the fifth material in Table 1 and can be exploited to simulate the responses of other materials.

3. Results

In this section, resonance frequencies measured on the undamaged plates are first presented. Thereafter, the FE model is identified by comparing the experimental and numerical modal displacements of the first mode. The effectiveness of the FE model is then shown through a comparison with the results of the fifth material with delamination.

3.1. Experimental Investigations on Intact Plates

Figure 6 shows the resultant first resonant frequencies of the undamaged plates as a function of the parameter $\frac{1}{2\pi a^2}\cdot\sqrt{\frac{TrD}{\rho\cdot h}}$.

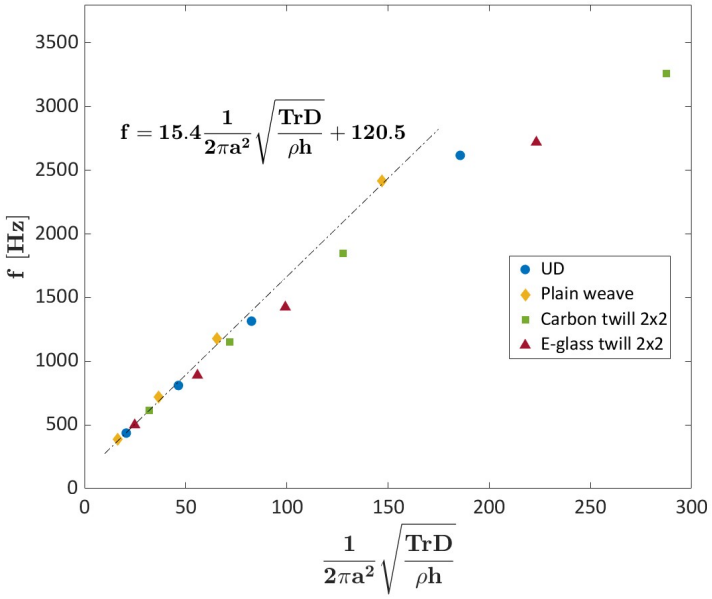

Figure 6. Measured frequencies as function of parameter $\frac{1}{2\pi a^2}\cdot\sqrt{\frac{TrD}{\rho\cdot h}}$.

As shown, for low values of the parameter $\frac{1}{2\pi a^2}\cdot\sqrt{\frac{TrD}{\rho\cdot h}}$, the measured frequencies are linearly dependent on the parameter according to Equation (3). When the parameter $\frac{1}{2\pi a^2}\cdot\sqrt{\frac{TrD}{\rho\cdot h}}$ has very high values, that is, for stiffer materials and smaller devices, the relationship deviates from the linearity with a decreasing slope, suggesting a change in the constraint provided by the device and, in turn, a change in the effectiveness of the device in isolating the mechanical vibrations. Focusing on the linear field, the slope λ is equal to 15.4, which suggests that the boundary conditions of the device approximate the condition of perfect clamping, although with some discrepancy, and are between the simply supporting and the clamping cases. The compliance of the rubber seal plays a key role in this regard, as also observed in previous investigations [20], given its noninfinite stiffness. It is also worth noting that the experimental results are linearly interpolated with a positive intercept equal to 120.5 Hz, which can be attributed to the in-plane spurious stresses induced by the vacuum clamping system, which increase the resultant frequencies. It is worth noting that, according to Figure 6, specific values for the slope and the intercept can be determined for each material, which can, accordingly, better describe the relationship between the first

resonant frequency and the parameter $\frac{1}{2\pi a^2} \cdot \sqrt{\frac{TrD}{\rho \cdot h}}$. However, since the goal is to identify an FE model that is generally valid, a global slope λ equal to 15.4 and a global intercept equal to 120.5 Hz were retained.

The deviation from the linearity shown In Figure 6 suggests that the constraint effectiveness, that is, the capacity to isolate the mechanical vibrations, depends on the material properties of the plate and on the size of the device. However, it must also be noted that the computation of the FRFs and, accordingly, of the first resonant frequency depends on the acquired signal. As the same input energy has been provided by the controlled impactor, the higher the flexural stiffness, the lower the resulting out-of-plane displacement, which, in turn, affects the FRF calculation. Figure 7 shows the acquired displacement signals and the resulting FRFs for the 50 × 50 mm device. In particular, Figure 7a reports the results of the unidirectional plate, Figure 7b presents the results of the plain weave plate, Figure 7c presents the results of the twill 2 × 2 carbon plate and Figure 7d presents the results for the twill 2 × 2 glass plate.

As shown in Figure 7, as the flexural stiffness increases, the out-of-plane displacement decreases, and the plate vibrations quickly end. In this regard, the damping properties of the material, which are mainly governed by the fiber volume fraction of the composite, also play a crucial role, affecting the peak broadening in the FRF. For the twill 2 × 2 carbon plate, the out-of-plane displacement is almost comparable with the measurement noise and, accordingly, the FRF does not show a clear and evident peak. According to Figure 7, the power amplitude of the signal must overcome the power amplitude due to the noise of at least one order of magnitude. It is worth noting that, with the vibrations of the twill 2 × 2 carbon plate consistently being limited over time, as shown in Figure 7c, a similar FRF would be obtained through a microphone. As such, the limited vibrations over time affect the computation of the first resonant frequency. As the material flexural stiffness increases, the impulse energy must increase in order to guarantee sufficient oscillations over time. This aspect also highlights that the inspected region size cannot be indefinitely reduced, and a compromise with the material flexural stiffness is necessary. It is also worth noting that, according to Figure 7, the reduction in the out-of-plane displacement as a result of the increasing stiffness implies that it becomes ever more comparable to the displacement at the extremities of the device. This aspect must be considered accordingly in the FE model of the local-IET test.

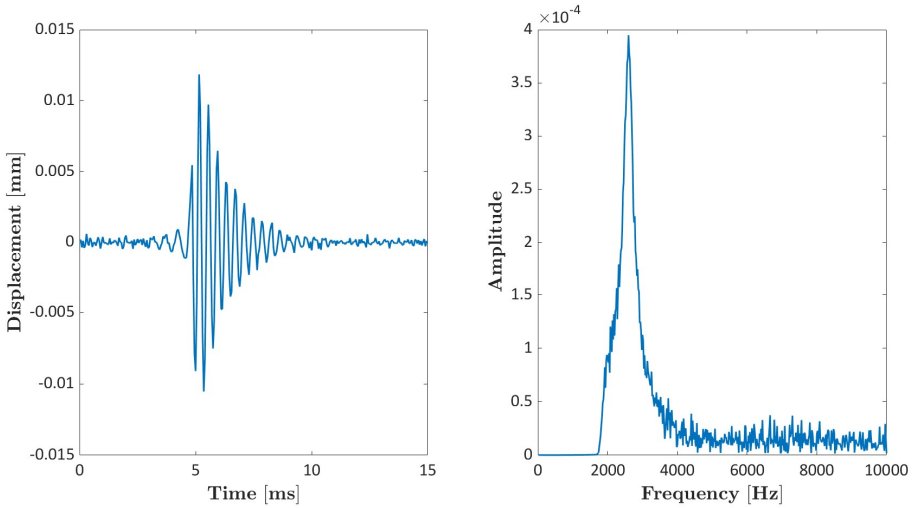

(**a**)

Figure 7. *Cont.*

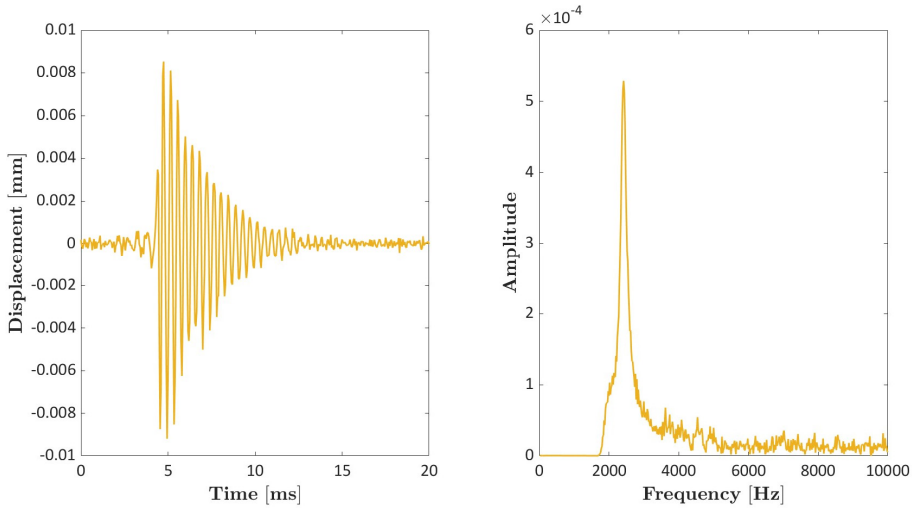

(**b**)

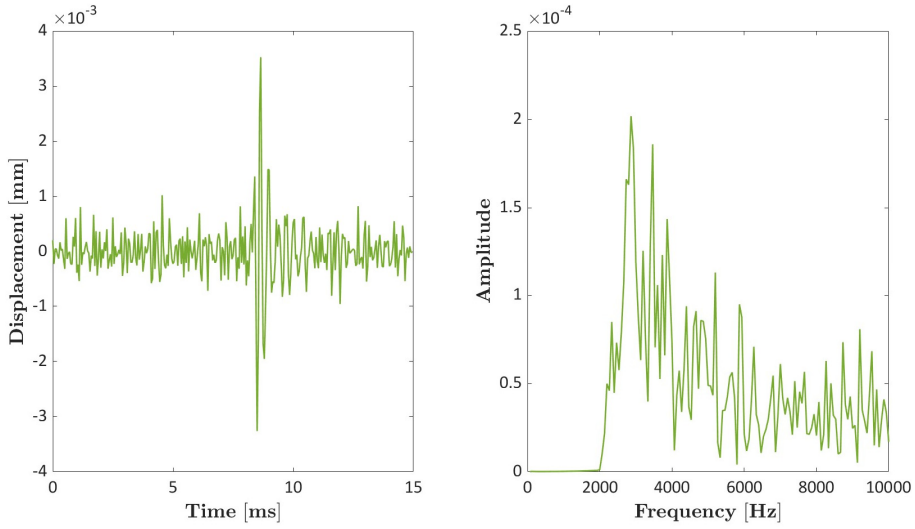

(**c**)

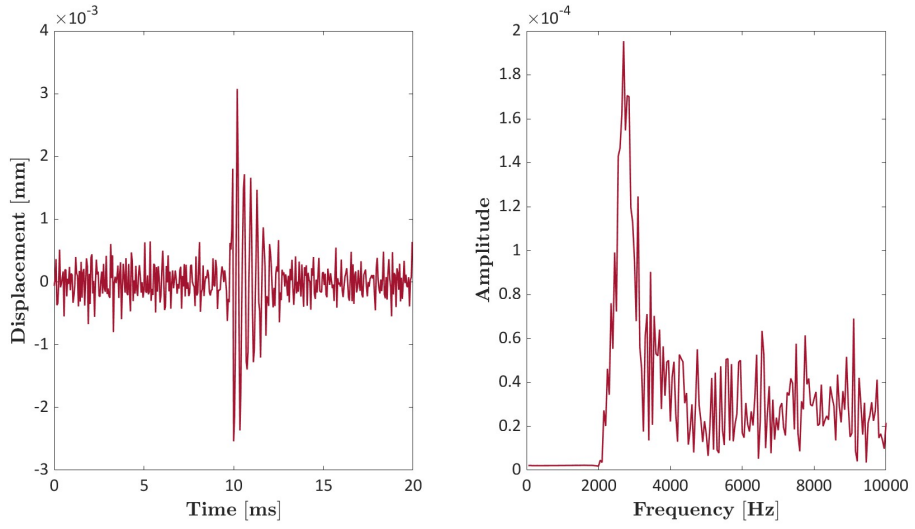

(**d**)

Figure 7. Displacement over time and FRFs in center of 50 × 50 mm device: (**a**) unidirectional plate; (**b**) plain weave plate; (**c**) twill 2 × 2 carbon plate; (**d**) twill 2 × 2 glass plate.

3.2. The Identification of the FE Model of the Local-IET Test

To replicate the local-IET test in the FE simulation environment, the stiffness of the springs was determined, such as the sum of the first resonant frequency of the FE model, and the intercept (120.5 Hz) matches the experimentally measured frequencies presented in the previous section. Table 2 reports the resulting stiffness of the FE model with translational springs and rotational springs. For the rotational springs model, the stiffness very slightly varied with the size of the device, and therefore, a unique mean value was considered. Nevertheless, the discrepancy between the experimentally measured frequencies and those calculated using the FE model was always lower than 5%.

Table 2. Resulting stiffnesses for FE model with translational and rotational springs.

Material	Size of the Device [mm]	First Resonant Frequency [Hz]	$k_{translational}$ [N/mm]	$k_{rotational}$ [N·mm/rad]
UD MAT#1	150 × 150	436	0.41	444
	100 × 100	810	1.28	
	75 × 75	1315	2.86	
	50 × 50	2617	7.95	
Plain Weave MAT#2	150 × 150	385	0.26	320
	100 × 100	719	0.89	
	75 × 75	1177	2.05	
	50 × 50	2418	6.16	
Twill 2 × 2 carbon fiber MAT#3	150 × 150	615	1.48	702
	100 × 100	1150	3.89	
	75 × 75	1847	7.84	
	50 × 50	3258	15.22	
Twill 2 × 2 glass fiber MAT#3	150 × 150	500	1.37	508
	100 × 100	890	3.24	
	75 × 75	1425	6.72	
	50 × 50	2720	16.5	

According to Table 2, the stiffness of the springs varies with the material elasticity and the size of the device in accordance with the previous observations. In this regard, we can consider that the higher the discrepancy between the displacements in the center and at the extremities of the device, the more the boundary conditions approximate the ideal clamping in accordance with the modal shape of the clamped solution. As such, the higher the material elasticity, the more comparable the displacements in the center and at the extremities, and the stiffness of the springs must decrease. Equivalently, the thinner the plate, the more the difference in displacements at the center and at the extremities, and the stiffness of the springs must increase to constrain the displacement in proximity to the extremities and resemble the perfectly clamped boundary conditions.

In order to identify the FE model that better replicates the local-IET tests, a comparison between the experimental and numerical modal displacements of the first mode was performed. The same measurement line inspected in the experimental investigations was extracted from the FE model. Figure 8 shows the comparison of the experimental and numerical modal displacements in the case of the plain weave plate and 150 × 150 mm device.

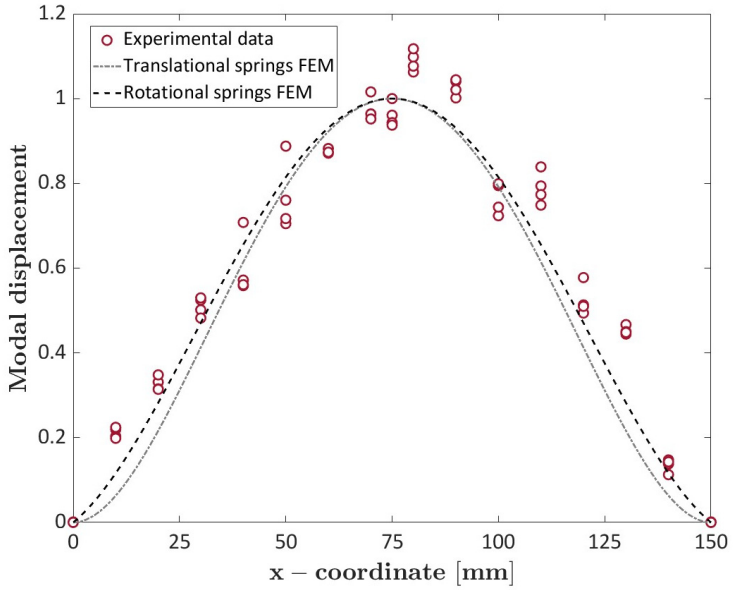

Figure 8. Experimental and numerical comparison of modal displacements for plain weave plate and 150 × 50 mm device: comparison with translational and rotational FE models.

For a consistent comparison, the modal displacements were normalized. As shown in Figure 8, although both models are in good agreement with the experimental data, the rotational springs model better predicts the vibrational response of the plate in correspondence with the boundaries, where the translational springs model shows a lower slope with respect to the experimental results. A similar conclusion can be achieved by comparing the experimental and numerical modal displacements of the unidirectional plate. Given the remarkable orthotropy of the material, the modal displacement was acquired along both the longitudinal and transverse directions. Figure 9a reports the experimental and numerical comparison for the translational springs model and the 75 × 75 mm device along the longitudinal and transverse materials directions, respectively. In Figure 9b, the comparison refers to the rotational springs model.

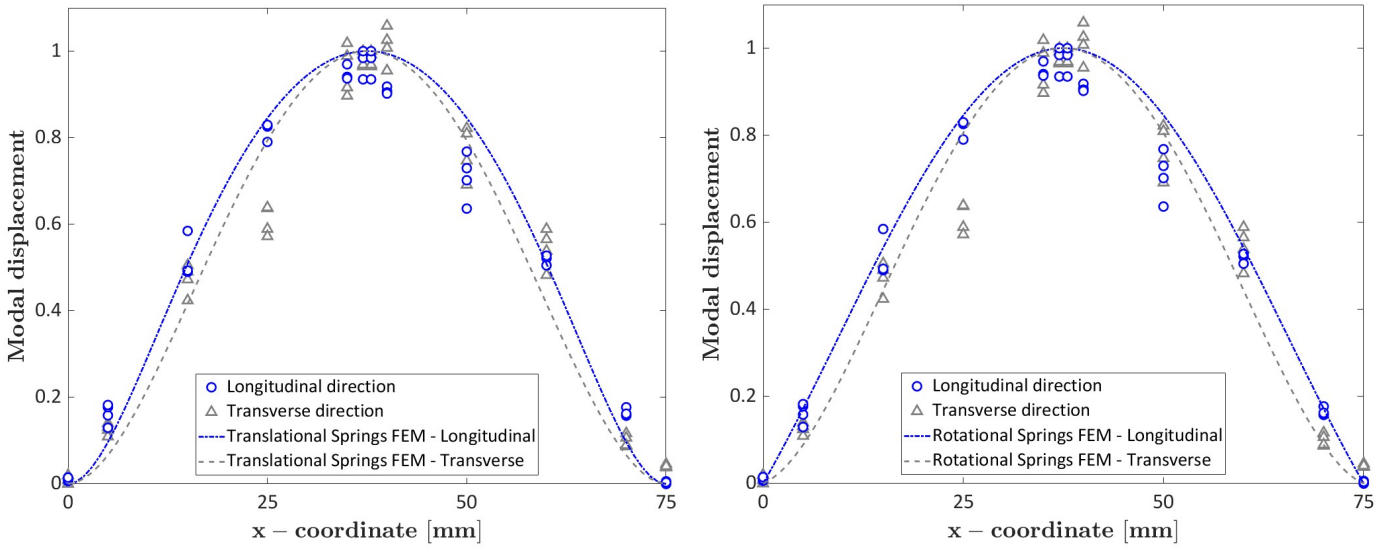

(**a**) (**b**)

Figure 9. Experimental and numerical comparisons of the modal displacements along the longitudinal and transverse directions of the unidirectional plate in the 75 × 75 mm device: (**a**) the translational FE model; (**b**) the rotational FE model.

By mapping along the transverse material direction, the experimental results present a flattening trend in correspondence of the extremities of the devices, while, along the longitudinal material direction, a more pronounced displacement is obtained in proximity to the extremities of the device. This consistently different behavior is well captured by the rotational springs model (Figure 9b). On the contrary, the translational springs model shows a flattening trend, even along the longitudinal direction, as a result of the constrained rotational degrees of freedom of the nodes at the boundaries. Considering the results of Figures 8 and 9, the rotational springs model better captures the vibrational response and was considered in the following.

In order to exploit the FE model to simulate the responses of the other materials, an optimization problem was formulated to extrapolate the relationship between the stiffness of the springs and the main parameters affecting the vibrational response, which are, according to Table 2, the material elasticity, i.e., the Tsai modulus, the plate thickness and the material density. The spring stiffness is therefore expressed as

$$k = w_1 \cdot TsaiM^{w_2} \cdot h^{w_3} \cdot \rho^{w_4} + w_5 \quad (5)$$

where the parameters $w = [w_1, w_2, w_3, w_4, w_5]$ were determined by formulating an optimization problem, which minimized the discrepancy between the values reported in Table 2 and the values calculated through Equation (5). The Nelder–Mead zero-order algorithm [33] was adopted. For the rotational springs model, it resulted in $w = [143.9, 0.3698, 0.669, -0.391, -346.6]$, which was used to compute the stiffness of the springs for the eight-layer glass fiber plate.

3.3. Validation on 8-Layer Glass Fiber Plate with Delamination

According to Equation (5), for the eight-layer glass fiber plate with the properties reported in Table 1 and the parameters determined in the previous section, the stiffness of the rotational springs is 207 Nmm/rad. The resulting FE first resonant frequency of the undamaged plate with the 100 × 100 mm device is 597 Hz, which is in very good accordance with the experimental average value of 601 Hz of the undamaged plate, as also assessed in [20].

The FE model was then compared to the experimental results obtained on the undamaged side of the glass fiber plate and with the delamination positioned in the center of the 100 × 100 mm device. The comparison of the experimental and numerical data is reported in Figure 10, where the ratio $\frac{\beta_{dam}}{\beta_{undam}}$ between the damaged and undamaged β factors is also represented with the red diamond markers.

The acquired values of β along the measurement line show a significant difference between the undamaged and damaged plates. Although a similar U-shaped trend is obtained in both cases, the β values of the delaminated plate are consistently higher than those of the undamaged plate. As a result of the nonlinearities due to the presence of the damage, the second mode doubles its contribution, as shown with the $\frac{\beta_{dam}}{\beta_{undam}}$ ratio in Figure 10. According to Figure 10, the FE model well captures the different behaviors of the undamaged and delaminated plates. The FE model can capture the trend and the increase in the β factor in the presence of delamination, and the excellent agreement between the experimental and numerical data proves its effectiveness.

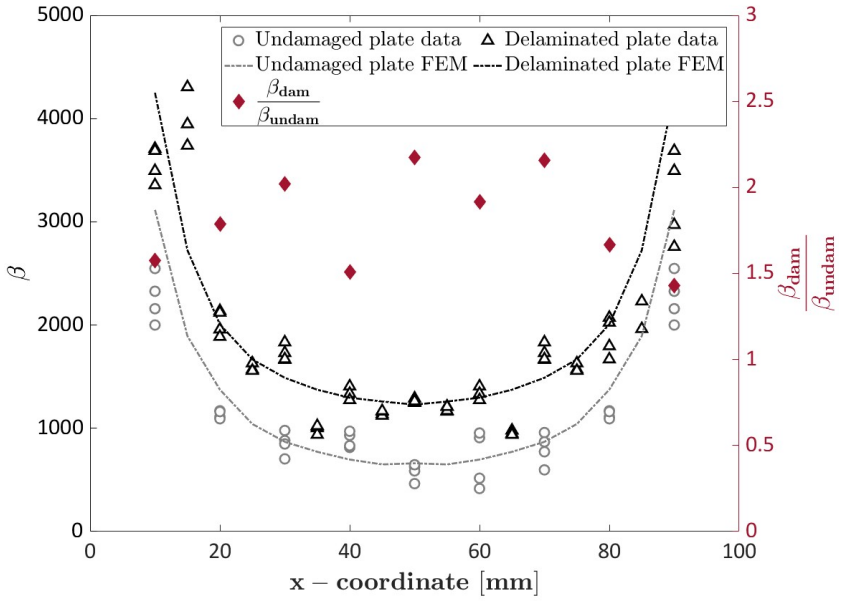

Figure 10. Comparison of experimental and numerical results: β factor for undamaged and delaminated plate and $\frac{\beta_{dam}}{\beta_{undam}}$ ratio between damaged and undamaged β factors.

4. Sensitivity Analysis to Delamination

To exploit the validated FE model of the local-IET test, a sensitivity analysis of the technique to detect delamination was addressed for an industrial composite material, indicated by *Leonardo S.p.A*. The material is made of unidirectional fiber laminae disposed with a quasi-stacking sequence for a total thickness of 3 mm. The analysis was conducted with the 150 × 150 mm clamping device, which was retained to provide an effective constraint for the investigated material. After exploiting the validated FE model, the predicted first and second resonant frequencies obtained were 672 Hz and 1130 Hz.

For the sensitivity analysis, different combinations of the position of the delamination, position of the impulse and size of the delamination were simulated in order to identify the best combination of impulse and delamination positions and to characterize the sensitivity to the delamination size. Given the symmetry of the model, the impulse position and delamination position were varied along a line passing through the center and parallel to one of the boundaries of the device. The impulse positions were 10 mm, 25 mm and 37 mm from the center of the device. The delamination was considered in the center and at 10 mm, 25 mm and 37 mm from the center of the device. It is worth noting that for the retained clamping device, the maximum modal displacement of the second mode occurred at 37 mm from the center. As such, it was expected that similar results would be obtained for the delamination positions farther than 37 mm from the center of the device. A rounded circular shape with a diameter varying between 5 mm and 50 mm, with intermediate values of 10 mm, 15 mm, 25 mm and 35 mm, is assumed for delamination. It is worth highlighting that, although delamination can have elliptical or non-rounded shapes [34,35], the rounded circular shape can be considered the smallest circle that can be inscribed within the elliptical or non-rounded delamination. Accordingly, through the rounded circular shape, we determined the lower bound of the sensitivity of the local-IET in the presence of delamination. For each position of the excitation impulse, a simulation with the undamaged plate was performed. As in the eight-layer glass fiber, the delamination was positioned in the neutral plane of the laminate.

For each simulation, in order to speed up the analysis without decreasing accuracy, the FRF was computed with a step size of 5 mm. The corresponding β factor and the ratio $\frac{\beta_{dam}}{\beta_{undam}}$ were computed for each point, and the maximum value of the $\frac{\beta_{dam}}{\beta_{undam}}$ ratio was used to assess the technique sensitivity. As in the region proximal to the boundaries, the modal displacement was almost null, thus challenging the accuracy of the experimental

acquisitions, and the identification of the maximum value of the $\frac{\beta_{dam}}{\beta_{undam}}$ ratio was restricted to the sub-domain with dimensions of 120 × 120 mm.

Figure 11 reports the trend of the maximum values of the $\frac{\beta_{dam}}{\beta_{undam}}$ ratio as a function of the delamination size.

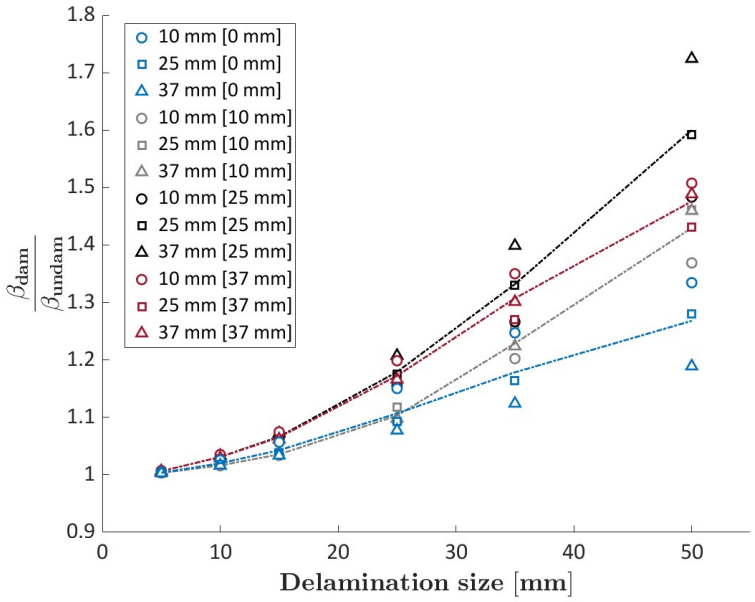

Figure 11. Results of the sensitivity analysis: maximum values of $\frac{\beta_{dam}}{\beta_{undam}}$ ratio for simulated configurations.

The different markers refer to the location of the impulse, while the different colors refer to the position of the delamination within the device, reported within square brackets. According to Figure 11, as the delamination size increases, the ratio $\frac{\beta_{dam}}{\beta_{undam}}$ increases, as shown with the dotted lines. In this regard, the local-IET has a good sensitivity in the presence of delamination, as an increment of 5% of the $\frac{\beta_{dam}}{\beta_{undam}}$ ratio is observed for a delamination size of 15 mm, which is only 1/10 of the device's dimensions. Furthermore, as the delamination moves from the center of the device, the $\frac{\beta_{dam}}{\beta_{undam}}$ ratio increases. Indeed, as the delamination moves from the center of the device, its influence on the second mode increases as well as the modal displacement of the second mode. However, the second-order nonlinear coefficient β accounts for the contributions of both the first and the second modes. Accordingly, at 25 mm from the center, the $\frac{\beta_{dam}}{\beta_{undam}}$ ratio reaches its maximum value. As such, differently from the 37 mm location, where the second mode is mainly affected by delamination, both the first and second modes are influenced by delamination at 25 mm from the center.

Finally, Figure 12 shows the maps of the $\frac{\beta_{dam}}{\beta_{undam}}$ ratio for a delamination size of 50 mm with an impulse provided at 10 mm from the center and for different positions of the delamination within the device. In particular, Figure 12a shows the $\frac{\beta_{dam}}{\beta_{undam}}$ map for the delamination located in the center of the device; in Figure 12b, the delamination is located at 10 mm from the center of the device; in Figure 12c, it is located at 25 mm; and in Figure 12d, it is located at 37 mm.

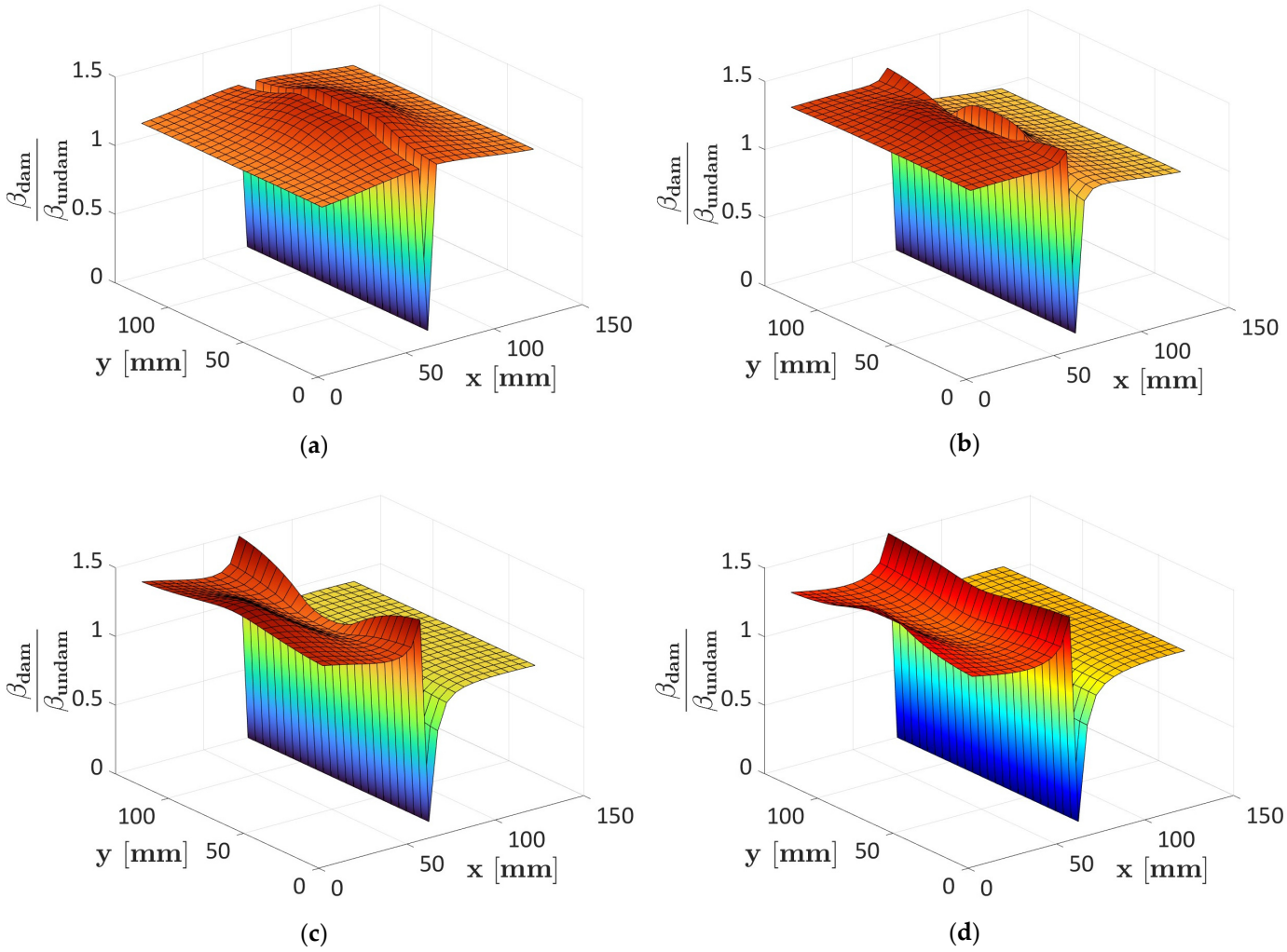

Figure 12. A map of the $\frac{\beta_{dam}}{\beta_{undam}}$ ratio for the delamination size of 50 mm and an impulse provided at 10 mm from the center: (**a**) delamination in the center; (**b**) delamination at 10 mm from the center; (**c**) delamination at 25 mm from the center; (**d**) delamination at 37 mm from the center of the device.

As shown in Figure 12, while in correspondence with the nodal line, the $\frac{\beta_{dam}}{\beta_{undam}}$ ratio is equivalently equal to zero, being here null the participation of the second mode, the map of the $\frac{\beta_{dam}}{\beta_{undam}}$ ratio, and, accordingly, the location of its maximum value, significantly varies according to the retained configuration. It is worth noting that a symmetric trend is obtained only in the case of delamination located in the center of the device. These considerations suggest that the $\frac{\beta_{dam}}{\beta_{undam}}$ ratio must be mapped within the whole inspected region in order to reliably identify the presence of delamination. Nevertheless, the consistent increase in the $\frac{\beta_{dam}}{\beta_{undam}}$ ratio from the unity confirms the good sensitivity of the local-IET to the detection of delamination. In this regard, it is worth remarking that in this work, the delamination was placed in the neutral plane of the laminate. Slight variations in the $\frac{\beta_{dam}}{\beta_{undam}}$ ratio can be expected when the delamination moves from the neutral plane, as observed by Zak et al. [25] on the natural frequencies of delaminated plates.

5. Conclusions

In this work, an innovative nondestructive methodology (local-IET) which allows for damage detection and quantification in composite plates was developed. The technique is based on the Impulse Excitation Technique (IET) and assesses the vibrational response of a local region of a component by clamping its boundaries through a specifically developed

device which exploits a vacuum to reversibly apply the constraint. From the vibrational response of the inspected region, the local material properties can be evaluated, and the technique was therefore referred to as local-IET.

In this work, we aimed to identify the Finite Element (FE) model of the nondestructive local-IET test to predict the first resonant frequency and the modal shape response of the composite plates subjected to the nondestructive test. By investigating four different composite plates with devices with dimensions of 50 × 50 mm, 75 × 75 mm, 100 × 100 mm and 150 × 150 mm, it was shown that the boundary conditions approximate the condition of perfect clamping, being between the simply supporting and the clamping cases. By investigating the modal displacement with a laser displacement sensor, we found that as the flexural stiffness increases or the device size decreases, the plate decreasingly vibrates over time, which, in turn, affects the computation of the resonances and of the Frequency Response Functions (FRFs). Accordingly, the inspected region size cannot be indefinitely reduced, and a compromise with the flexural stiffness is necessary. The constraint provided by the device was modeled in the FE environment with translational springs and with rotational springs at the extremities. The comparison with the experimental measurements of the modal displacement on the undamaged plates showed that the rotational springs model better captures the vibrational response.

The FE model was then validated on an eight-layer glass fiber plate with a circular delamination with a 50 mm diameter. The experimental investigations with a 100 × 100 mm device showed that the local-IET can successfully assess the presence of delamination, as the second-order nonlinear coefficient β, defined as the ratio between the power amplitude of the second resonance frequency and the squared power amplitude of the first resonance frequency doubles its value between the undamaged and the delaminated conditions. As a result of the nonlinearities due to the presence of damage, the second mode contribution increases. An excellent agreement was observed between the experimental and numerical data, proving the effectiveness of the FE model.

Finally, by exploiting the validated FE model, a sensitivity analysis on the detection of delamination was carried out by varying the size of the delamination, which was assumed to be of a circular shape, its position within the device and the position of the impulse. The sensitivity analysis was addressed for an industrial composite material, indicated by *Leonardo S.p.A*, with the 150 × 150 mm device. The results show that the local-IET has a good sensitivity in the presence of delamination, with a 5% increase in the β even for a delamination size of 15 mm, i.e., 1/10 of the device. Also, we found the maximum sensitivity of the local-IET for the delamination positioned between the maxima of the first and second modes' modal displacements, although not with a remarkable difference with respect to the other investigated positions. In order to reliably identify the presence of delamination with the local-IET, we suggest mapping the β factor within the whole inspected region.

In conclusion, given its simplicity and relatively low-cost equipment, the methodology has the potential to be easily translated in the industrial world, with the additional advantage of providing quantitative information on the health state of the composite structure. The presented FE model, validated with experimental results, also allows the sensitivity of the local-IET to other damage mechanisms of composites to be investigated to design the clamping device for the material of interest, once the signal noise and damping properties are properly accounted for, and to define acceptable damage levels for the identification of maintenance strategies of composite components.

Author Contributions: Conceptualization, C.B.N. and A.T.; methodology, C.B.N. and A.T.; validation, P.P.; formal analysis, P.P.; investigation, P.P.; data curation, P.P.; writing—original draft preparation, C.B.N. and P.P.; writing—review and editing, A.T., M.B., and D.S.P.; supervision, M.B., F.A., and D.S.P.; project administration, D.S.P. All authors have read and agreed to the published version of the manuscript.

Funding: This research received no external funding.

Institutional Review Board Statement: Not applicable.

Informed Consent Statement: Not applicable.

Data Availability Statement: The raw data supporting the conclusions of this article will be made available by the authors on request.

Conflicts of Interest: Authors M. Boccaccio and F. Acerra were employed by the company Leonardo S.p.A. The remaining authors declare that the research was conducted in the absence of any commercial or financial relationships that could be construed as a potential conflict of interest.

References

1. Boccaccio, M.; Malfense Fierro, G.P.; Meo, M.; Bolton, G. Development and Focusing Enhancement of Nonlinear Air-Coupled Acoustic Technique for Damage Characterization in Materials. *Mater. Today Proc.* **2021**, *34*, 266–274. [CrossRef]
2. Böhm, R.; Hufenbach, W. Experimentally Based Strategy for Damage Analysis of Textile-Reinforced Composites under Static Loading. *Compos. Sci. Technol.* **2010**, *70*, 1330–1337. [CrossRef]
3. Toyama, N.; Takatsubo, J. Lamb Wave Method for Quick Inspection of Impact-Induced Delamination in Composite Laminates. *Compos. Sci. Technol.* **2004**, *64*, 1293–1300. [CrossRef]
4. Su, Z.; Ye, L.; Lu, Y. Guided Lamb Waves for Identification of Damage in Composite Structures: A Review. *J. Sound Vib.* **2006**, *295*, 753–780. [CrossRef]
5. Sai, B.; Talreja, R. Damage Classification Based on Stiffness Reduction in Cross-Ply Laminates with Convolution Neural Networks. In *SPIE—The International Society for Optical Engineering—Sensors and Smart Structures Technologies for Civil, Mechanical, and Aerospace Systems*; SPIE: Bellingham, WA, USA, 2022.
6. Sai, B.; Talreja, R. Analysis of Lamb Wave Propagation in Cross-Ply Laminates Modeled with Homogenized Properties of Transverse Cracked Plies. In *SPIE—The International Society for Optical Engineering—Nondestructive Characterization and Monitoring of Advanced Materials, Aerospace, Civil Infrastructure, and Transportation XVI*; SPIE: Bellingham, WA, USA, 2022.
7. Tridello, A.; D'Andrea, A.; Paolino, D.S.; Belingardi, G. A Novel Methodology for the Assessment of the Residual Elastic Properties in Damaged Composite Components. *Compos. Struct.* **2017**, *161*, 435–440. [CrossRef]
8. Libonati, F.; Vergani, L. Damage Assessment of Composite Materials by Means of Thermographic Analyses. *Compos. B Eng.* **2013**, *50*, 82–90. [CrossRef]
9. Harizi, W.; Chaki, S.; Bourse, G.; Ourak, M. Mechanical Damage Assessment of Polymer-Matrix Composites Using Active Infrared Thermography. *Compos. B Eng.* **2014**, *66*, 204–209. [CrossRef]
10. Pieczonka, L.; Aymerich, F.; Brozek, G.; Szwedo, M.; Staszewski, W.J.; Uhm, T. Modelling and Numerical Simulations of Vibrothermography for Impact Damage Detection in Composites Structures. *Struct. Control Health Monit.* **2012**, *20*, 626–638. [CrossRef]
11. Abry, J.C.; Choi, Y.K.; Chateauminois, A.; Dalloz, B.; Giraud, G.; Salvia, M. In-Situ Monitoring of Damage in CFRP Laminates by Means of AC and DC Measurements. *Compos. Sci. Technol.* **2001**, *61*, 855–864. [CrossRef]
12. Raihan, R.; Adkins, J.M.; Baker, J.; Rabbi, F.; Reifsnider, K. Relationship of Dielectric Property Change to Composite Material State Degradation. *Compos. Sci. Technol.* **2014**, *105*, 160–165. [CrossRef]
13. Fazzino, P.D.; Reifsnider, K.L.; Majumdar, P. Impedance Spectroscopy for Progressive Damage Analysis in Woven Composites. *Compos. Sci. Technol.* **2009**, *69*, 2008–2014. [CrossRef]
14. Vadlamudi, V.; Shaik, R.; Raihan, R.; Reifsnider, K.; Iarve, E. Identification of Current Material State in Composites Using a Dielectric State Variable. *Compos. Part A Appl. Sci. Manuf.* **2019**, *124*, 105494. [CrossRef]
15. Garnier, C.; Pastor, M.L.; Eyma, F.; Lorrain, B. The Detection of Aeronautical Defects in Situ on Composite Structures Using Non Destructive Testing. *Compos. Struct.* **2011**, *93*, 1328–1336. [CrossRef]
16. Ambu, R.; Aymerich, F.; Ginesu, F.; Priolo, P. Assessment of NDT Interferometric Techniques for Impact Damage Detection in Composite Laminates. *Compos. Sci. Technol.* **2006**, *66*, 199–205. [CrossRef]
17. Boursier Niutta, C.; Tridello, A.; Paolino, D.S.; Belingardi, G. Residual Properties in Damaged Laminated Composites through Nondestructive Testing: A Review. *Materials* **2021**, *14*, 4513. [CrossRef]
18. Boursier Niutta, C.; Tridello, A.; Belingardi, G.; Paolino, D.S. Nondestructive Determination of Local Material Properties of Laminated Composites with the Impulse Excitation Technique. *Compos. Struct.* **2021**, *262*, 113607. [CrossRef]
19. Boursier Niutta, C. Enhancement of a New Methodology Based on the Impulse Excitation Technique for the Nondestructive Determination of Local Material Properties in Composite Laminates. *Appl. Sci.* **2020**, *11*, 101. [CrossRef]
20. Boursier Niutta, C. Residual Elastic Response in Damaged Woven Laminates through Local Impulse Excitation Technique. *Compos. Struct.* **2022**, *293*, 115723. [CrossRef]
21. Talreja, R.; Phan, N. Assessment of Damage Tolerance Approaches for Composite Aircraft with Focus on Barely Visible Impact Damage. *Compos. Struct.* **2019**, *219*, 1–7. [CrossRef]
22. Talreja, R. Manufacturing Defects in Composites and Their Effects on Performance. In *Polymer Composites in the Aerospace Industry*; Elsevier: Amsterdam, The Netherlands, 2019; pp. 83–97, ISBN 9780081026793.

23. Matthews, F.L. Damage in Fibre-Reinforced Plastics; Its Nature, Consequences and Detection. In Proceedings of the 3rd International Conference on Damage Assessment of Structures (DAMAS 99), Dublin, Ireland, 28–30 June 1999; Volume 168, pp. 1–16.
24. Schoeppner, G.A.; Abrate, S. Delamination Threshold Loads for Low Velocity Impact on Composite Laminates. *Compos. Part. A Appl. Sci. Manuf.* **2000**, *31*, 903–915. [CrossRef]
25. Zak, A.; Krawczuk, M.; Ostachowicz, W. Numerical and Experimental Investigation of Free Vibration of Multilayer Delaminated Composite Beams and Plates. *Comput. Mech.* **2000**, *26*, 309–315. [CrossRef]
26. *ASTM E1876-22*; Standard Test Method for Dynamic Young's Modulus, Shear Modulus, and Poisson's Ratio by Impulse Excitation of Vibration. ASTM International: West Conshohocken, PA, USA, 2015.
27. Tsai, S.W.; Melo, J.D.D. An Invariant-Based Theory of Composites. *Compos. Sci. Technol.* **2014**, *100*, 237–243. [CrossRef]
28. Hearmon, R.F.S. The Frequency of Flexural Vibration of Rectangular Orthotropic Plates with Clamped or Supported Edges. *J. Appl. Mech.* **1959**, *26*, 537–540. [CrossRef]
29. Hong, X.; Liu, Y.; Lin, X.; Luo, Z.; He, Z. Nonlinear Ultrasonic Detection Method for Delamination Damage of Lined Anti-Corrosion Pipes Using PZT Transducers. *Appl. Sci.* **2018**, *8*, 2240. [CrossRef]
30. Boursier Niutta, C.; Ciardiello, R.; Tridello, A.; Paolino, D.S. Epoxy and Bio-Based Epoxy Carbon Fiber Twill Composites: Comparison of the Quasi-Static Properties. *Materials* **2023**, *16*, 1601. [CrossRef]
31. Livermore Software Technology Corporation (LSTC). *LSTC LS-DYNA Keyword User's Manual Volume I*; Livermore Software Technology Corporation (LSTC): Livermore, CA, USA, 2017; ISBN 978-3-540-23882-9.
32. Livermore Software Technology Corporation (LSTC). *LSTC LS-DYNA Keyword User's Manual Volume II*; Livermore Software Technology Corporation (LSTC): Livermore, CA, USA, 2017; ISBN 978-3-540-23882-9.
33. Nelder, J.A.; Mead, R. A Simplex Method for Function Minimization. *Comput. J.* **1965**, *7*, 308–313. [CrossRef]
34. Aymerich, F.; Dore, F.; Priolo, P. Prediction of Impact-Induced Delamination in Cross-Ply Composite Laminates Using Cohesive Interface Elements. *Compos. Sci. Technol.* **2008**, *68*, 2383–2390. [CrossRef]
35. Aymerich, F.; Dore, F.; Priolo, P. Simulation of Multiple Delaminations in Impacted Cross-Ply Laminates Using a Finite Element Model Based on Cohesive Interface Elements. *Compos. Sci. Technol.* **2009**, *69*, 1699–1709. [CrossRef]